An evaluation of vertical mixing parameterization of ocean boundary layer turbulence for cohesive sediments

Jinliang Liu[a], Jianguo Yuan[a], Jun-Hong Liang[a,b,c,*]

[a] *Department of Oceanography & Coastal Sciences, Louisiana State University, Baton Rouge, 70803, LA, USA*
[b] *Center for Computation and Technology, Louisiana State University, Baton Rouge, 70803, LA, USA*
[c] *Coastal Coastal Studies Institute, Louisiana State University, Baton Rouge, 70803, LA, USA*

ABSTRACT

Accurate parameterization for both diffusivity and turbulent kinetic energy (TKE) dissipation rate is important for the simulation of reactive tracers such as cohesive sediments. We implemented a second-order closure parameterization for mixing in ocean surface boundary layer in the Coupled Ocean-Atmosphere-Wave-Sediment Transport (COAWST) model. The parameterization is more suitable than the existing parameterizations in the COAWST model for the modeling of cohesive sediments: It includes the wave-driven Langmuir turbulent effect, a more complete pressure strain covariance parameterization in the eddy viscosity and diffusivity, and also TKE dissipation rate. Solutions using a one-dimensional configuration are compared to solutions using a three-dimensional model that simulates the ocean surface boundary layer turbulence and size distributions of flocs of different sizes. The result shows that the simulation using the newly implemented parameterization reproduces fairly well the profiles of vertical eddy viscosity,

*Corresponding author: Jun-Hong Liang, jliang@lsu.edu

TKE dissipation rate, total mass concentration of suspended sediment, and mass averaged settling velocity in wave-driven Langmuir turbulence. The water depth dependence of floc size distribution is also reproduced in the one-dimensional model. In addition, the result based on the standard $k - \omega$ model mostly underestimates (up to $\sim$90%) the averaged settling velocity of suspended sediments in the water column. The result also suggests that misrepresentation of Langmuir turbulence effect in vertical mixing parameterization could cause substantial biases in the forecast/hindcast transport model for cohesive sediment.

1. Introduction

Turbulent mixing in the ocean surface boundary layer (OSBL), a thin (usually tens to a few hundred meters deep) buffer layer between the atmosphere and ocean interior, mediates the air-sea exchange of momentum, heat, and gas fluxes, and is critical for the global climate and marine ecosystem. It greatly influences the upper ocean dynamics and is essential for altering the large-scale ocean circulation, the distribution of temperature and salinity, and the dispersion and transportation of materials with different buoyancy (e.g. Smith et al., 2016; Liang et al., 2018; Kukulka, 2020). Therefore, an accurate prediction of the role of the upper ocean under a changing climate and the influence of anthropogenic activities requires a better representation of turbulent mixing in the OSBL.

In the earth system model and operational ocean model, however, vertical mixing is generally not resolved explicitly but parameterized, i.e. represented by a physics-based mathematical model dependent on flow variables and surface forcing with a small number of empirical parameters, because of three main reasons as follows. Firstly, it is not feasible to resolve all the scales for computation of turbulent flows in the climate model and hindcast/forecast model under the present technique condition in the most state-of-the-art High-Performance Computing systems (Fox-Kemper et al., 2014, 2019). As a result, most realistic ocean models have a grid resolution coarser than the one required for simulating OSBL turbulence. Secondly, even in a high-resolution version of a small computational domain, the hydrostatic approximation applied in these models prevents their capabilities of simulating three-dimensional turbulence. Thirdly, these models which use finite-difference or finite-volume schemes have advantages of efficiency and flexibility in realistic oceanic applications, nevertheless, they are less accurate in calculating the horizontal gradients than the pseudo-spectral models commonly utilized in the turbulence computing model in the OSBL (e.g. Sullivan and McWilliams, 2010).

The OSBL turbulence is predominantly driven by meteorological conditions near the ocean surface, including winds, heating and cooling, and surface gravity waves (e.g. D'Asaro, 2014). It is also modulated by the earth's rotation (e.g. Liu et al., 2018), horizontal density stratification (e.g. Fan et al., 2018), and horizontal currents (e.g. Yuan and Liang, 2021). Particularly, the interaction between surface gravity waves and wind-driven mean current drives Langmuir turbulence, which is characterized by the counter-rotating vortices roughly aligned with the downwind direction and often marked by the surface congregated zone (windrows) of sargassum, droplets, and gas bubbles. In the coastal oceans and continental shelf regions, Langmuir turbulence can extend throughout the water column, sweeping the non-attached macroalgae into streaks near the seabed in the shelf region and is also responsible for suspension events of sediments by observations (e.g. Gargett et al., 2004; Dierssen et al., 2009). During the suspension of the sediments, water-column turbulence also alters the size and spatial distributions of cohesive sediments through flocculation processes (Liu et al., 2019).

The flocculation process includes aggregation and breakup of cohesive sediments (fine-grained compound containing silt, clay, fine sand, and organic substance), through which sediment flocs (an agglomeration of mineral/organic matter) of different sizes are constructed and demolished (see a two-dimensional schematic for flocculation processes in Langmuir turbulence in Fig. 1). Aggregation refers to the process during which smaller aggregates and primary mineral particles bond together forming flocs (e.g. Mehta, 2013; Strom and Keyvani, 2016), and its rate varies with particle size, salinity, pH, and the particle collision frequency (e.g. Winterwerp, 1998; Burd and Jackson, 2009; Mietta et al., 2009). Breakup refers to the process that parent flocs are separated into smaller daughter flocs (or primary particles) by inter-particle collision (Dyer, 1989) or turbulent shear. Flocculation processes not only add more uncertainties in determining the properties of cohesive sediments, such as the settling velocity, shape, size, composition, and density, of cohesive sediment (e.g. Liss et al., 2004; Strom and Keyvani, 2011; Mehta, 2013), but also play an important role in modulating the concentration of suspended sediments carried by turbulent eddies (e.g. Droppo et al., 1998; Verney et al., 2011; Sherwood et al., 2018; Liu et al., 2019).

Through a series of laboratory and field experiments (e.g. Braithwaite et al., 2012; Keyvani and Strom, 2014; Strom and Keyvani, 2016), progress has been made in understanding the relationship between flocculation processes and the turbulent shear rate (defined as $G = \sqrt{\epsilon/\nu} = \nu/\eta^2$, with ϵ the turbulent kinetic energy dissipation rate, ν the kinematic viscosity, and η the Kolmogorov length scale (Kolmogorov, 1941)). Turbulence enhances the growth and breakup rate of flocs by increasing inter-particle collision and increasing the shear stress exerted on the floc, respectively. This means accurate information of turbulent mixing is necessary to better understand the cohesive sediment transport associated with flocculation processes. Recently, using a numerical model that simultaneously computes turbulence and flocs of different sizes, Liu et al. (2019) showed that Langmuir turbulence suspends and organizes flocs of different sizes in the water column. It also increases the aggregation and breakup rates of flocs that are located in similar regions with high turbulent dissipation rates and restrains those of others. They also showed that floc size distribution varies with depth and floc mass concentration profiles change with floc size in wave-driven Langmuir turbulence. Although there is no doubt that Langmuir turbulence plays an important role in modulating the transport of cohesive sediments, such turbulence-resolving simulations are computationally prohibitive in sediment transport models for realistic oceans (e.g. Fox-Kemper et al., 2019) and the effect of boundary layer turbulence on vertical mixing has to be parameterized in those models.

There are two classes of vertical mixing parameterizations: first-order closure and second-order closure. One of the commonly used first-order closures is the K-profile parameterization (KPP) proposed by Large et al. (1994). In the KPP, the eddy viscosity and diffusivity are modeled as the product of a dimensionless shape function, a length scale that represents boundary layer depth, and a turbulent velocity scale in the boundary layer. Sinha et al. (2015) proposed a modified KPP for shallow seas, by replacing the constant velocity scale in the KPP with a new velocity scale that is a function of dimensionless vertical coordinate, in addition to a counter-gradient term that accounts for nonlocal transport. It is convenient to implement the KPP in forecast/hindcast models since there is no additional prognostic equation to solve. However, neither the KPP nor its modified variants (e.g. Sinha et al., 2015) provides direct information on the turbulent kinetic energy dissipation rate, which is an important factor in modeling flocculation processes (e.g. Liu et al., 2019). Therefore it is not suitable for a cohesive sediment transport model that incorporates the flocculation model. One of the popular second-order closure, also called second-moment closure (SMC), schemes is the one proposed by Mellor and Yamada (1982) (referred to as MY2.5 hereafter). The MY2.5 parameterization and its variants (e.g. Umlauf et al., 2003) are also widely used in regional ocean circulation models. This model adds two prognostic equations, including one for turbulent kinetic energy and the other for the product of turbulent kinetic energy and turbulent length scale, to determine the eddy viscosity and diffusivity. The drawback of the MY2.5 model is that it does not consider the enhancement in vertical mixing due to Langmuir turbulence. Kantha and Clayson (2004) (referred to as KC04 hereafter) proposed a modified MY2.5 model that incorporates the effect of Langmuir turbulence in the transport equations of turbulent kinetic energy and turbulent length scale, by adding a Stokes production term that is the product of the Reynolds stress and the Stokes drift shear. But the KC04 model does not consider the effect of Craik–Leibovich (CL) vortex force on stability functions. Harcourt (2013, 2015) rederived the Reynolds transport equations for turbulent momentum flux and buoyancy flux from the Boussinesq Navier-Stokes equation that includes the CL vortex force. In their models, an additional component of vertical momentum flux that is directed down the gradient of the Stokes drift is added to the algebraic Reynolds stress model. However, the examination of the performance by the modified SMC models was usually for stably stratified conditions in deep water, and their performance in the neutrally stratified shallow ocean is not yet clear. Another drawback in MY2.5 model is the incomplete parameterization of pressure covariance (e.g. Canuto et al., 2001). Recently, Yu et al. (2018) proposed a modified SMC model ($k-\omega$ model) that includes the influence of Langmuir turbulence in the transport equations of turbulent kinetic energy and turbulent frequency as well as stability functions, in addition to a modification on the pressure covariance.

Recently, turbulence parameterizations have been examined using profiles of currents, temperature, and salinity (Van Roekel et al., 2018; Li et al., 2019; Liang et al., 2022), but not for reactive tracers such as cohesive sediments. In particular, to our best knowledge, no study has examined the performance of vertical mixing parameterization of Langmuir turbulence in modeling cohesive sediment transport with flocculation processes. The specific objectives of this study are (1) to develop a one-dimensional vertical

(1DV) sediment transport model, which resolves the floc size and concentration distributions in the water column, and (2) to assess the accuracy of a modified vertical mixing parameterization that includes the effect of Langmuir turbulence in cohesive sediment transport. Since direct observational evaluation of the vertical mixing parameterization of Langmuir turbulence on the cohesive sediment transport is currently lacking, we conduct coupled-turbulence-sediment simulation using a large-eddy simulation model (LES) embedded with a size-resolved floc model for cohesive sediment transport under the same initial and forcing condition as applied in the 1DV model. A Large eddy simulation model resolves the large-scale turbulent structure and parameterizes subgrid-scale motions since most of the energy and turbulent fluxes in the flow is contained in the former (Sullivan et al., 1994). The LES model used in this study is the National Center for Atmospheric Research Large Eddy Simulation model, which has been widely applied to study OSBL turbulence driven by different atmospheric and wave conditions (e.g. Sullivan and McWilliams, 2010). The flocculation model embeded in the LES model has been verified with the published laboratory experiment data and more details including the description of the LES model can be found in Liu et al. (2019). Since LES models resolve OSBL turbulence yet excludes all other larger-scale processes, their solutions are commonly used as the truth to develop and improve parameterizations for vertical mixing in the OSBL (e.g. Van Roekel et al., 2012; Reichl et al., 2016) and air-sea fluxes (e.g. Liang et al., 2013). The rest of the paper is organized as follows. Section 2 describes the 1DV model and its configuration. Section 3 presents the results of a benchmark model run using 1DV model, which includes flocculation processes, the effect of wave-driven Langmuir turbulence, and wave breaking. The comparison of solutions between 1DV and LES model is also discussed, with the conclusions drawn in Section 4.

2. Model description and configuration

2.1. Model description

The three-dimensional transport equation for the mass concentration (unit: $\mathrm{g\,L^{-1}}$) of suspended sediments is as follows

$$\frac{\partial C_i}{\partial t} = \frac{\partial uC_i}{\partial x} + \frac{\partial vC_i}{\partial y} + \frac{\partial wC_i}{\partial z} - \frac{\partial w_{s,i}C_i}{\partial z} + \frac{\partial}{\partial z}(K_C\frac{\partial C_i}{\partial z}) \overbrace{+\mathcal{G}_{ag}(i) + \mathcal{G}_{bs}(i) + \mathcal{G}_{bc}(i) - \mathcal{L}_{ag}(i) - \mathcal{L}_{bs}(i) - \mathcal{L}_{bc}(i)}^{\text{flocculation processes}}, \tag{1}$$

where the first three terms on the RHS of equation (1) indicate the advection terms along the three directions (x, y, z), respectively, with (u, v, w) the corresponding velocity components. The fourth and fifth terms on the RHS describe the temporal variation in mass concentration due to turbulent diffusion and settling of sediment, respectively; C_i and $w_{s,i}$ are the mass concentration and settling velocity of sediment in size class i, respectively; and K_C is the vertical eddy diffusivity of sediment. The last six terms on the RHS indicate the changes due to flocculation processes ($\mathcal{G}$ and $\mathcal{L}$ represent the gain and loss of mass, respectively), where ag, bs, and bc denote the processes of aggregation, breakup due to turbulent shear, and breakup due to collision, respectively.

By assuming horizontal homogeneity and negelecting the vertical advection, equation (1) could be reduced to the following one-dimensional format:

$$\frac{\partial C_i}{\partial t} = -\frac{\partial w_{s,i} C_i}{\partial z} + \frac{\partial}{\partial z}(K_C \frac{\partial C_i}{\partial z}) + \text{flocculation processes}, \qquad (2)$$

where the implementation of flocculation processes shown in the last term on the RHS of equation (2) was based on a population balance model, the FLOCMOD (Verney et al., 2011), in the Coupled Ocean-Atmosphere-Wave-Sediment Transport (COAWST) modeling framework, following Sherwood et al. (2018). The vertical eddy diffusivity of suspended sediment (K_C) is computed based on a modified $k-\omega$ model for vertical mixing, which considered the effect of Langmuir turbulence (Yu et al., 2018), as described in the following section.

2.2. Modified turbulence second-moment closure model

The effect of Langmuir turbulence on vertical mixing is incorporated by adding a production term related to the shear of Stokes drift in the transport equations of turbulent kinetic energy and turbulent frequency, in addition to a modification on pressure covariance when deriving stability functions (Yu et al., 2018). The transport equation of turbulent kinetic energy is calculated as follows:

$$\frac{\partial k}{\partial t} = \frac{\partial}{\partial z}(\frac{K_M}{\sigma_k}\frac{\partial k}{\partial z}) - (\overline{u'w'}(\frac{\partial \overline{u}}{\partial z} + \frac{\partial u^{St}}{\partial z}) + \overline{v'w'}(\frac{\partial \overline{v}}{\partial z} + \frac{\partial v^{St}}{\partial z})) + \overline{w'b'} - \epsilon, \qquad (3)$$

where $k=\frac{1}{2}(\overline{u'^2}+\overline{v'^2}+\overline{w'^2})$ is the turbulent kinetic energy, K_M is the eddy viscosity, σ_k is the Schmidt number for turbulent kinetic energy, and ϵ is the turbulent kinetic energy dissipation rate.

The transport equation of turbulence frequency is calculated as follows:

$$\frac{\partial\omega}{\partial t}=\frac{\partial}{\partial z}(\frac{K_M}{\sigma_\omega}\frac{\partial\omega}{\partial z})-\frac{\omega}{k}(c_{\hat{\omega}_1}(\overline{u'w'}\frac{\partial\overline{u}}{\partial z}+\overline{v'w'}\frac{\partial\overline{v}}{\partial z})+c_{\hat{\omega}_4}(\overline{u'w'}\frac{\partial u^{St}}{\partial z}+\overline{v'w'}\frac{\partial v^{St}}{\partial z}))+c_{\hat{\omega}_3}\overline{w'b'}-c_{\hat{\omega}_2}\epsilon, \tag{4}$$

where ω is the characteristic turbulence frequency (Kolmogorov, 1941), and σ_ω is the Schmidt number for turbulent frequency. In this study, we use $\sigma_k=\sigma_\omega=2.0$, $c_{\hat{\omega}_1}=1.9$, $c_{\hat{\omega}_2}=3.1$, and $c_{\hat{\omega}_4}=4.1$. It should be noted that the values of $c_{\hat{\omega}_1}$, $c_{\hat{\omega}_2}$, and $c_{\hat{\omega}_4}$ in Yu et al. (2018) are different from the ones used in this study, which are obtained through trial and error with the best match of eddy viscosity profile to the LES solution. The buoyancy production terms in equations (3) and (4) are ignored in this study since the focus is on the neutrally stratified condition following Liu et al. (2019).

The turbulent momentum fluxes, buoyancy flux, and sediment flux are computed as

$$\overline{u'w'}=-(K_M\frac{\partial\overline{u}}{\partial z}+K_M^{St}\frac{\partial u^{St}}{\partial z}), \tag{5}$$

$$\overline{v'w'}=-(K_M\frac{\partial\overline{v}}{\partial z}+K_M^{St}\frac{\partial v^{St}}{\partial z}), \tag{6}$$

$$\overline{w'b'}=-K_N\frac{\partial\overline{B}}{\partial z}, \tag{7}$$

$$\overline{w'C'}=-K_C\frac{\partial\overline{C}}{\partial z}, \tag{8}$$

with

$$K_M=k\tau S_M, \tag{9}$$

$$K_M^{St}=k\tau S_M^{St}, \tag{10}$$

$$K_N = k\tau S_N, \quad (11)$$

$$K_C = k\tau S_C, \quad (12)$$

where $\tau = k/\epsilon$ is the eddy turnover time, K_M and K_M^{St} are the eddy viscosity for mean flow and Stokes drift, respectively, and K_N and K_C are the eddy diffusivities for scalars and sediment concentration, respectively. The calculation of dimensionless numbers including S_M,S_M^{St}, S_N, and S_C is included in the appendix.

2.3. Model configuration

The 1DV model was implemented on a 4 by 4 grid in the horizontal direction, with 80 grids in the vertical direction. Spatially uniform forcing was applied on the top of the computational domain, along with doubly periodic open boundary conditions. The water depth (h) is 15 m.

At the bottom, the seabed is assumed erodible. Erosion flux ($E_{s,i}$) is calculated following Ariathurai and Arulanandan (1978):

$$E_{s,i} = E_0(1-\phi)\frac{\tau_{sf} - \tau_{cr,i}}{\tau_{cr,i}}, \text{if } \tau_{sf} > \tau_{cr,i} \quad (13)$$

where for each floc size bin i, E_s is the surface erosion mass flux ($\mathrm{kg\,m^{-2}\,s^{-1}}$), E_0 is the bed erodibility ($\mathrm{kg\,m^{-2}\,s^{-1}}$), ϕ is the porosity, τ_{cr} is the critical shear stress (Pa) calculated following Soulsby et al. (1997), and τ_{sf} is the total skin friction bottom stress (Pa) calculated following Warner et al. (2008). The fraction of each sediment class is evaluated from published in-situ observation in an inner-shelf region (Law et al., 2008), and interpolated into each size bin.

At the ocean surface, the wind speed at 10 m above the surface is $10\,\mathrm{m\,s^{-1}}$, corresponding to a wind stress of $0.159\,\mathrm{N\,m^{-2}}$, and a surface friction velocity (u_*) of $0.0126\ \mathrm{m\,s^{-1}}$.

The Stokes drift $u^{St}(z)$ is calculated based on linear wave theory (Lentz and Fewings, 2012). A series of simulations are conducted to assess the effect of different vertical parameterizations on floc size and spatial distributions and are summarized in Table 1. The benchmark experiment (Case 1DVa) includes flocculation processes and is driven by surface wind stress. The effect of Langmuir turbulence is included by implementing a modified $k-\omega$ model for vertical mixing (section 2.2). The effect of wave breaking is also incorporated using the parameterization by Craig and Banner (1994). Cases 1DVb and 1DVc are the experiments using standard $k-\omega$ model (Umlauf et al., 2003) following the implementation by Warner et al. (2005), with and without wave breaking, respectively. Case 1DVd has the same setup with the benchmark experiment but excludes the flocculation processes. Fifteen cohesive sediment classes were included on a logarithmic equal-distance grid, ranging from 4.0 μm to 2048.0 μm (19 size classes), with the fractal dimension $N_f = 2.0$. These flocs had densities ranging from 2600.0 $\mathrm{kg\,m^{-3}}$ to 1028.1 $\mathrm{kg\,m^{-3}}$ and settling velocities ranging from 0.013 $\mathrm{mm\,s^{-1}}$ to 6.86 $\mathrm{mm\,s^{-1}}$ (see Table 2). The initial concentration of sediment is zero for all size classes. All the simulations start from a spin-up run without sediment.

3. Model results

The effect of boundary layer turbulence on vertical mixing is represented by eddy viscosity (K) in forecast/hindcast ocean models. By assuming a constant Schmidt number, the eddy diffusivity for sediments can be obtained if eddy viscosity is given. In addition, the turbulent shear rate (G), which controls the aggregation and breakup rate of flocs, is dependent on turbulent kinetic energy dissipation rate (ϵ) (Sherwood et al., 2018; Liu et al., 2019). Therefore, the improvement in the prediction of cohesive sediment transport in turbulent flows needs accurate modeling of eddy viscosity and dissipation rate, if turbulence is not resolved. In this section, the solutions from the 1DV model were compared to those from the LES model (Liu et al., 2019) to assess the applicability of the 1DV model.

The profile of eddy viscosity from the LES solution is diagnosed as follows,

$$K = \frac{|\langle u'_{\parallel} w \rangle|}{|\partial_z \langle u^L_{\parallel} \rangle|}, \tag{14}$$

where $\langle u'_{\parallel} w \rangle$ is the Reynolds stress and $\langle u^L_{\parallel} \rangle = \langle u_{\parallel} \rangle + \langle u^{St}_{\parallel} \rangle$ is the Lagrangian mean velocity. The subscript $\parallel$ denotes the horizontal components.

Fig. 2 shows the vertical profiles of normalized eddy viscosity ($K/(u_* |h|)$) and normalized turbulent kinetic energy dissipation rate ($\epsilon/(u_* |h|)$) in the 1DV model and the LES model. The K profile diagnosed from the LES model is approximately symmetric about $z/|h| =$-0.6, and has a longer tail near the sea surface than that near the seabed (Fig. 2a). The magnitude of eddy viscosity in Case 1DVa is twice as large as that in the LES model above $z/|h| =$-0.4 and below $z/|h| =$-0.7, and the location of the maximum K is similar in both models. However, when using the empirical parameters ($c_{\hat{\omega_1}} = c_{\hat{\omega_4}} = 0.555$, and $c_{\hat{\omega_2}} = 0.833$) suggested by Yu et al. (2018), the magnitude of K in the 1DV model is much smaller than that in the LES model throughout the water column (not shown). The magnitude of maximum K in Cases 1DVb and 1DVc is only 25% of that in the LES model, despite that the magnitude of K near both boundaries is similar. The presence of wave breaking greatly increases the turbulent dissipation rate (ϵ) near the surface (Fig. 2b). The magnitude of ϵ in Case 1DVa is slightly larger than that in the LES model, and ϵ decays more slowly in the former than that in the latter.

Fig. 3 shows the vertical profiles of normalized mean horizontal velocity (U/u_*) and normalized total floc mass concentration ($C_s/C_{s,v}$, where C_s is the total mass concentration of sediments and subscript v denotes the vertical average) in the 1DV model and the LES model. The normalized mean horizontal velocity in Case 1DVa is larger than that in the LES model near the surface ($z/|h| >$-0.2) and the seabed ($z/|h| <$-0.9) (Fig. 3a). In contrast, the normalized mean horizontal velocity in Cases 1DVb and 1DVc is larger than that in the LES model throughout the water column. In addition, the normalized mean horizontal velocity in the 1DV models decreases with depth. This is different from the velocity profile in the LES model, where there is a slight increase in the normalized mean horizontal velocity in the middle of the water column. As explained in Tejada-Martinez and Grosch (2007), the increase in alongwind velocity with depth in the middle of the water column is the combined effect of a thinner bottom boundary in the downwelling branch of Langmuir circulations (LCs) and the thicker bottom boundary in upwelling branches of LCs. The lack of representation of the upwelling/downwelling branches of LCs is likely the cause that along wind velocity decrease monotonically water depth in all the 1DV simulations. Without flocculation processes, the normalized total floc mass concentration

($C_s/C_{s,v}$) in Case 1DVd (Fig. 3b) is vertically more uniform compared to those in other cases. With flocculation processes, the normalized total floc mass concentration in the benchmark run (Case 1DVa) is more uniform than those in Case 1DVb and 1DVc, which has a much larger value near the seabed than that in the LES model.

The vertical profile of floc mass density is shown in Fig. 4. In the benchmark run (Case 1DVa), the median floc size in the middle of the water column is larger than that near the surface and seabed (Fig. 4a), due to the relatively low dissipation rate (Fig. 2b), which is also reported in the LES model result by Liu et al. (2019). In addition, due to stronger simulated vertical mixing (Fig. 2a), the mass concentration in the middle of the water column in Case 1DVa is larger than those in Cases 1DVb (Fig. 4b) and 1DVc (Fig. 4c). It is also obvious that the median floc size reduces near the surface in Case 1DVc (Fig. 4c) compared to that in Case 1DVb (Fig. 4b) since wave breaking is included in the former. This is also observed in the LES model result by Liu et al. (2019). Without flocculation processes, there is no mass exchange across sediment of different size classes (Case 1DVd, Fig. 4d).

Fig. 5 shows the vertical profiles of normalized floc mass concentration ($C_i/(C_{i,v})$) in individual size bin in the 1DV model and the LES model. For $D = 4.0\,\mu$m, the profile of normalized floc mass concentration in Cases 1DVb and 1DVc is larger than that in Case 1DVa near the seabed (Fig. 5a), but is smaller than that in Case 1DVa in the upper column. For $D = 128.0\,\mu$m, the lower value of normalized floc mass concentration in Cases 1DVb and 1DVc compared to that in Case 1DVa (Fig. 5b) is because less sediments are transported to the surface due to relative weak vertical mixing in the former.

For $D = 1024.0\,\mu$m, the normalized floc mass concentration in Cases 1DVb and 1DVc has a local peak near the seabed (Fig. 5c) while it is larger in the middle of the water column in Case 1DVa. The results suggest inaccurate vertical mixing parameterization causes large biases in vertical profiles of floc mass concentration in individual size bin.

Settling velocity is one of the key factors in cohesive sediment transport modeling (e.g. Dyer, 1989; Sherwood et al., 2018). It also determines the residence time of sediment particles in the water column (Burd and Jackson, 2009). Different from the noncohesive sediment of which settling velocity is primarily affected by the physical properties including particle size, shape, and density (e.g. Dietrich, 1982; Rubey, 1933; Ferguson and Church, 2004), settling velocity of cohesive sediment is also modulated by the flocculation processes. In order to examine the effect of different vertical mixing parameterizations on the settling velocity of total suspended sediment, fig. 6 shows the comparison of mass weighted settling velocity W_s (see equation (21) in Liu et al., 2019) between the 1DV model and the LES model. Among all the cases, the result based on the modified $k-\omega$ model (case 1DVa) overall performs better than the others in terms of capturing the shape and magnitude of W_s profile compared to the LES solution, although all the 1DV cases underestimate the W_s in the middle of the water column. There is also a substantial decrease in W_s near the surface in Cases 1DVb and 1DVc, which is also indicated by the less concentration of larger flocs near the surface ($z/|h| >$ -0.2) in Fig. 4b,c. In contrast, without flocculation processes, W_s is more uniform throughout the water column. In addition, the result based on the standard $k - \omega$ model (case 1DVb) suggests that if applied in a forecast/hindcast transport model for cohesive sediment, it's likely that the averaged setting velocity of suspended sediment will be largely underestimated, which leads to a longer residence time of suspended sediment in the water column and a much longer distance for transport by horizontal currents. The result also suggests that the misrepresentation of vertical mixing parameterization leads to substantial errors (as much as ∼50% in the mid-depth and ∼90% near the surface under the simulated condition) in the averaged settling velocity.

4. Conclusions

In this study, we implement an improved vertical mixing parameterization for OSBL mixing, based on a second-moment closure ($k - \omega$) model that accounts for the effect of Langmuir turbulence (Yu et al., 2018), in the COAWST modeling framework (Sherwood et al., 2018) with the addition of a size-based flocculation model (FLOCMOD, Verney et al., 2011). The model is applied in a one-dimensional (1DV) setting to simulate the vertical transport of cohesive sediment in wave-driven Langmuir turbulence, with a benchmark run that includes nineteen size classes of cohesive sediment with the inclusion of flocculation processes and wave breaking. By comparing the solutions between the 1DV model and solutions from a Large Eddy Simulation (LES) model (Liu et al., 2019) under the same initial and forcing condition, the performance of vertical mixing parameterization for vertical transport of cohesive sediment is evaluated. The major findings of this study are summarized as follows:

(1) The results show that the 1DV model with the modified $k - \omega$ model based on Yu et al. (2018) reasonably regenerates the profiles of vertical eddy viscosity and dissipation rate in wave-driven Langmuir turbulence, with a more uniform profile of total floc mass concentration compared to that in the LES model.

(2) The 1DV model using the standard $k - \omega$ model for vertical mixing overall underestimates (up to 90%) the average settling velocity of cohesive sediment compared to that in the LES model under the simulated condition.

(3) The water depth dependence of the floc size distribution is also observed in the 1DV model, similar to that reported in the turbulence-resolving floc simulation study (Liu et al., 2019).

(4) The results also show that inaccurate modeling of vertical mixing causes substantial biases in the floc size distribution, vertical profile of floc mass concentration, and averaged settling velocity. Therefore, the effect of Langmuir turbulence needs to be considered and incorporated into forecast/hindcast models for cohesive sediment transport to accurately represent the size and concentration distribution of the cohesive sediments in the water column.

There are a few interesting directions for future research that require more collaborative effort in the modeling community. For example, the evaluation of existing vertical mixing parameterizations of Langmuir turbulence for cohesive sediment transport has not been conducted in a three-dimensional configuration but is essential to a complete assessment of mixing schemes.

Three-dimensional heterogeneous turbulence can redistribute the cohesive sediments in both horizontal and vertical directions and modify their setting velocity and size distribution by modulating the flocculation processes (Liu et al., 2019). In addition, the winds and waves are assumed in the same direction in this study, and the misalignment between the two observed in the real ocean (e.g. Yoshikawa et al., 2018; McWilliams et al., 2014) is not considered. Although not considered in the modified $k-\omega$ model by Yu et al. (2018), this can be improved by including the effect of misaligned wind and wave on the profile of eddy viscosity in the vertical mixing parameterization following the recent practice in the KPP model (Solano and Fan, 2022). Finally, while the 1DV model in this study is tested for cohesive sediment with flocculation processes, the same modeling framework can also be applied to study other reactive tracers, e.g. spilled oil (e.g. Aiyer et al., 2019; Cui et al., 2021) and gas bubbles (e.g. Liang et al., 2012), whose physical properties (e.g. size, shape, and density) are also modulated by the similar aggregation and breakup processes due to turbulent shear, and relevant assessment of existing vertical mixing parameterization is needed and critical to better constrain the associated transport modeling.

Acknowledgements

JY and JHL were supported by the National Science Foundation through grant OCE-1945502. Computations were performed using supercomputers at Louisiana State University, and at Louisiana Optical Network Infrastructure (LONI).

Appendix A Parameters in the modified $k-\omega$ model

The dimensionless stability functions used to determine the vertical eddy viscosity and diffusivity in equations (9)-(12) are calculated as follows

$$S_M = \frac{\xi_1\xi_6 + \xi_2\xi_4}{\xi_3\xi_6 - \xi_2\xi_5}, \tag{A.1}$$

$$S_M^{St} = \frac{\xi_1\xi_5 + \xi_3\xi_4}{\xi_3\xi_6 - \xi_2\xi_5}, \tag{A.2}$$

$$S_C = S_N = \frac{\xi_7 + \xi_8 S_M + \xi_9 S_M^{St}}{\xi_{10}}, \tag{A.3}$$

where

$$\xi_1 = \frac{\lambda_1}{2} + \lambda_4(\frac{\lambda_2 + 3\lambda_3}{3} + \frac{\lambda_6 + \lambda_7}{2}) S_N G_N, \tag{A.4}$$

$$\xi_2 = \frac{1}{12}[(\lambda_2^2 - 9\lambda_3^2) G_V + (\lambda_2^2 + 18\lambda_2\lambda_3 + 9\lambda_3^2) Gs], \tag{A.5}$$

$$\xi_3 = 1 - \lambda_4 G_N - \frac{1}{3}(\lambda_2^2 - 3\lambda_3^2) G_M - \frac{1}{12}(7\lambda_2^2 + 18\lambda_2\lambda_3 + 15\lambda_3^2) G_V - \frac{1}{4}(\lambda_2^2 - \lambda_3^2) G_S, \tag{A.6}$$

$$\xi_4 = \frac{\lambda_1}{2} + \lambda_4(\frac{\lambda_2 - 3\lambda_3}{3} + \frac{\lambda_6 - \lambda_7}{2}) S_N G_N, \tag{A.7}$$

$$\xi_5 = \frac{1}{12}[(\lambda_2^2 - 18\lambda_2\lambda_3 + 9\lambda_3^2) G_M + (\lambda_2^2 - 9\lambda_3^2) G_V], \tag{A.8}$$

$$\xi_6 = 1 - \lambda_4 G_N - \frac{1}{3}(\lambda_2^2 - \lambda_3^2) G_M - \frac{1}{12}(7\lambda_2^2 - 18\lambda_2\lambda_3 + 15\lambda_3^2) G_V - \frac{1}{3}(\lambda_2^2 - 3\lambda_3^2) G_S, \tag{A.9}$$

$$\xi_7 = \frac{2}{3}, \tag{A.10}$$

$$\xi_8 = (\frac{\lambda_6 - \lambda_7}{2} + \frac{\lambda_2 - 3\lambda_3}{3}) G_M + (\frac{\lambda_6 + \lambda_7}{2} + \frac{\lambda_2 + 3\lambda_3}{3}) G_V, \tag{A.11}$$

$$\xi_9 = (\frac{\lambda_6 - \lambda_7}{2} + \frac{\lambda_2 - 3\lambda_3}{3}) G_V + (\frac{\lambda_6 + \lambda_7}{2} + \frac{\lambda_2 + 3\lambda_3}{3}) G_S, \tag{A.12}$$

$$\xi_{10} = 1 - (\frac{4}{3}\lambda_4 + \lambda_8) G_N - \frac{1}{4}(\lambda_6^2 - \lambda_7^2)(G_M + G_S) - \frac{1}{2}(\lambda_6^2 + \lambda_7^2) G_V. \tag{A.13}$$

For more details on the derivation of stability functions and coefficients, the reader is referred to appendix B in Yu et al. (2018).

The dimensionless shear number (G_M, G_S, G_V) and buoyancy number (G_N) are given as follows (Yu et al., 2018):

$$G_M = \tau^2[(\frac{\partial \overline{u}}{\partial z})^2 + \frac{\partial \overline{v}}{\partial z})^2], \tag{A.14}$$

$$G_S = \tau^2[(\frac{\partial u^{St}}{\partial z})^2 + \frac{\partial v^{St}}{\partial z})^2], \tag{A.15}$$

$$G_V = \tau^2[\frac{\partial \overline{u}}{\partial z}\frac{\partial u^{St}}{\partial z} + \frac{\partial \overline{v}}{\partial z}\frac{\partial v^{St}}{\partial z}], \tag{A.16}$$

$$G_N = -\tau^2 N^2, \tag{A.17}$$

where $N^2 = \frac{\partial \overline{B}}{\partial z}$ is the square of the buoyancy frequency. Other parameters used in equations (A.4)-(A.13) include $\lambda_1 = \frac{4a_1}{c_1}$, $\lambda_2 = \frac{2a_2}{c_1}$, $\lambda_3 = \frac{2a_3}{c_1}$, $\lambda_4 = \frac{4a_4}{c_1}$, $\lambda_6 = \frac{a_{b1}}{c_{b1}}$, $\lambda_7 = \frac{a_{b2}}{c_{b1}}$, $a_1 = \frac{2}{3} - \frac{c_2}{2}$, $a_2 = 1 - \frac{c_3}{2}$, $a_3 = 1 - \frac{c_4}{2}$, $a_4 = \frac{1}{2} - \frac{c_5}{2}$, $a_{b1} = 1 - c_{b2}$, $a_{b2} = 1 - c_{b3}$, $a_{b3} = 2$, $a_{b4} = 2(1 - c_{b5})$, $c_1 = 5.0$, $c_2 = 0.6983$, $c_3 = 1.9664$, $c_4 = 1.094$, $c_5 = 0.495$, $c_{b1} = 5.6$, $c_{b2} = 0.6$, $c_{b3} = 1$, $c_{b4} = 0$, and $c_{b5} = 0.3333$.

References

Aiyer, A., Yang, D., Chamecki, M., Meneveau, C., 2019. A population balance model for large eddy simulation of polydisperse droplet evolution. J. Fluid Mech. 878, 700–739.

Ariathurai, R., Arulanandan, K., 1978. Erosion rates of cohesive soils. J. Hydraul. Div. 104, 279–283.

Braithwaite, K., Bowers, D., Nimmo Smith, W., Graham, G., 2012. Controls on floc growth in an energetic tidal channel. J. Geophys. Res. Oceans 117.

Burd, A.B., Jackson, G.A., 2009. Particle aggregation. Annu. Rev. Mar. Sci. 1, 65–90.

Canuto, V.M., Howard, A., Cheng, Y., Dubovikov, M., 2001. Ocean turbulence. part i: One-point closure model—momentum and heat vertical diffusivities. J. Phys. Oceanogr. 31, 1413–1426.

Craig, P.D., Banner, M.L., 1994. Modeling wave-enhanced turbulence in the ocean surface layer. J. Phys. Oceanogr. 24, 2546–2559.

Cui, L., Harris, C.K., Tarpley, D.R., 2021. Formation of oil-particle-aggregates: Numerical model formulation and calibration. Front. Mar. Sci. 8, 629476.

D'Asaro, E.A., 2014. Turbulence in the upper-ocean mixed layer. Annu. Rev. Mar. Sci. 6, 101–115.

Dierssen, H., Zimmerman, R.C., Drake, L.A., Burdige, D.J., 2009. Potential export of unattached benthic macroalgae to the deep sea through wind-driven langmuir circulation. Geophys. Res. Lett. 36.

Dietrich, W.E., 1982. Settling velocity of natural particles. Water Resour. Res. 18, 1615–1626.

Droppo, I., Walling, D., Ongley, E., 1998. Suspended sediment structure: implications for sediment and contaminant transport modelling. IAHS-AISH publ. , 437–444.

Dyer, K., 1989. Sediment processes in estuaries: future research requirements. J. Geophys. Res. Oceans 94, 14327–14339.

Fan, Y., Jarosz, E., Yu, Z., Rogers, W.E., Jensen, T.G., Liang, J.H., 2018. Langmuir turbulence in horizontal salinity gradient. Ocean Model. 129, 93–103. doi:https://doi.org/10.1016/j.ocemod.2018.07.010.

Ferguson, R., Church, M., 2004. A simple universal equation for grain settling velocity. J. Sediment. Res. 74, 933–937.

Fox-Kemper, B., Adcroft, A., Böning, C.W., Chassignet, E.P., Curchitser, E., Danabasoglu, G., Eden, C., England, M.H., Gerdes, R., Greatbatch, R.J., Griffies, S.M., Hallberg, R.W., Hanert, E., Heimbach, P., Hewitt, H.T., Hill, C.N., Komuro, Y., Legg, S., Le Sommer, J., Masina, S., Marsland, S.J., Penny, S.G., Qiao, F., Ringler, T.D., Treguier, A.M., Tsujino, H., Uotila, P., Yeager, S.G., 2019. Challenges and prospects in ocean circulation models. Front. Mar. Sci. 6. doi:10.3389/fmars.2019.00065.

Fox-Kemper, B., Bachman, S., Pearson, B., Reckinger, S., 2014. Principles and advances in subgrid modelling for eddy-rich simulations. Clivar Exchanges 19, 42–46.

Gargett, A., Wells, J., Tejada-Martinez, A., Grosch, C., 2004. Langmuir supercells: A mechanism for sediment resuspension and transport in shallow seas. Science 306, 1925–1928.

Harcourt, R.R., 2013. A second-moment closure model of langmuir turbulence. J. Phys. Oceanogr. 43, 673–697.

Harcourt, R.R., 2015. An improved second-moment closure model of langmuir turbulence. J. Phys. Oceanogr. 45, 84–103.

Kantha, L.H., Clayson, C.A., 2004. On the effect of surface gravity waves on mixing in the oceanic mixed layer. Ocean Model. 6, 101–124.

Keyvani, A., Strom, K., 2014. Influence of cycles of high and low turbulent shear on the growth rate and equilibrium size of mud flocs. Mar. Geol. 354, 1–14.

Kolmogorov, A.N., 1941. The local structure of turbulence in incompressible viscous fluid for very large reynolds numbers. Cr Acad. Sci. URSS 30, 301–305.

Kukulka, T., 2020. Horizontal transport of buoyant material by turbulent jets in the upper ocean. J. Phys. Oceanogr. 50, 827–843.

Large, W.G., McWilliams, J.C., Doney, S.C., 1994. Oceanic vertical mixing:

A review and a model with a nonlocal boundary layer parameterization. Rev. Geophys. 32, 363–403.

Law, B.A., Hill, P., Milligan, T., Curran, K., Wiberg, P., Wheatcroft, R., 2008. Size sorting of fine-grained sediments during erosion: results from the western gulf of lions. Cont. Shelf Res. 28, 1935–1946.

Lentz, S.J., Fewings, M.R., 2012. The wind-and wave-driven inner-shelf circulation. Annu. Rev. Mar. Sci. 4, 317–343.

Li, Q., Reichl, B.G., Fox-Kemper, B., Adcroft, A.J., Belcher, S.E., Danabasoglu, G., Grant, A.L., Griffies, S.M., Hallberg, R., Hara, T., et al., 2019. Comparing ocean surface boundary vertical mixing schemes including langmuir turbulence. J. Adv. Model. Earth Syst. 11, 3545–3592.

Liang, J.H., Deutsch, C., McWilliams, J.C., Baschek, B., Sullivan, P.P., Chiba, D., 2013. Parameterizing bubble-mediated air-sea gas exchange and its effect on ocean ventilation. Glob. Biogeochem. Cycles. 27, 894–905.

Liang, J.H., McWilliams, J.C., Sullivan, P.P., Baschek, B., 2012. Large eddy simulation of the bubbly ocean: New insights on subsurface bubble distribution and bubble-mediated gas transfer. J. Geophys. Res. Oceans 117.

Liang, J.H., Wan, X., Rose, K.A., Sullivan, P.P., McWilliams, J.C., 2018. Horizontal dispersion of buoyant materials in the ocean surface boundary layer. J. Phys. Oceanogr. 48, 2103–2125. doi:10.1175/JPO-D-18-0020.1.

Liang, J.H., Yuan, J., Wan, X., Liu, J., Liu, B., Jang, H., Tyagi, M., 2022. Exploring the use of machine learning to parameterize vertical mixing in the ocean surface boundary layer. Ocean Model. doi:10.1016/j.ocemod.2022.102059.

Liss, S.N., Droppo, I.G., Leppard, G.G., Milligan, T.G., 2004. Flocculation in natural and engineered environmental systems. CRC press.

Liu, J., Liang, J.H., McWilliams, J.C., Sullivan, P.P., Fan, Y., Chen, Q., 2018. Effect of planetary rotation on oceanic surface boundary layer turbulence. J. Phys. Oceanogr. 48, 2057–2080.

Liu, J., Liang, J.H., Xu, K., Chen, Q., Ozdemir, C.E., 2019. Modeling sediment flocculation in langmuir turbulence. J. Geophys. Res. Oceans 124, 7883–7907. doi:https://doi.org/10.1029/2019JC015197.

McWilliams, J.C., Huckle, E., Liang, J., Sullivan, P.P., 2014. Langmuir turbulence in swell. J. Phys. Oceanogr. 44, 870–890. doi:10.1175/JPO-D-13-0122.1.

Mehta, A.J., 2013. An introduction to hydraulics of fine sediment transport. volume 38. World Scientific Publishing Company.

Mellor, G.L., Yamada, T., 1982. Development of a turbulence closure model for geophysical fluid problems. Rev. Geophys. 20, 851–875.

Mietta, F., Chassagne, C., Manning, A.J., Winterwerp, J.C., 2009. Influence of shear rate, organic matter content, ph and salinity on mud flocculation. Ocean Dyn. 59, 751–763.

Reichl, B.G., Wang, D., Hara, T., Ginis, I., Kukulka, T., 2016. Langmuir turbulence parameterization in tropical cyclone conditions. J. Phys. Oceanogr. 46, 863–886.

Rubey, W.W., 1933. Settling velocity of gravel, sand, and silt particles. Am. J. Sci. , 325–338.

Sherwood, C.R., Aretxabaleta, A.L., Harris, C.K., Rinehimer, J.P., Verney, R., Ferré, B., 2018. Cohesive and mixed sediment in the regional ocean modeling system (roms v3. 6) implemented in the coupled ocean-atmosphere-wave-sediment transport modeling system (coawst r1234). Geosci. Model Dev. 11, 1849–1871.

Sinha, N., Tejada-Martínez, A.E., Akan, C., Grosch, C.E., 2015. Toward a k-profile parameterization of langmuir turbulence in shallow coastal shelves. J. Phys. Oceanogr. 45, 2869–2895. doi:10.1175/JPO-D-14-0158.1.

Smith, K.M., Hamlington, P.E., Fox-Kemper, B., 2016. Effects of submesoscale turbulence on ocean tracers. J. Geophys. Res. Oceans .

Solano, M., Fan, Y., 2022. A new k-profile parameterization for the ocean surface boundary layer under realistic forcing conditions. Ocean Model. , 101958.

Soulsby, R., Whitehouse, R., et al., 1997. Threshold of sediment motion in coastal environments, in: Pacific Coasts and Ports' 97: Proceedings of the 13th Australasian Coastal and Ocean Engineering Conference and the 6th Australasian Port and Harbour Conference; Volume 1, Centre for Advanced Engineering, University of Canterbury. p. 145.

Strom, K., Keyvani, A., 2011. An explicit full-range settling velocity equation for mud flocs. J. Sediment. Res. 81, 921–934.

Strom, K., Keyvani, A., 2016. Flocculation in a decaying shear field and its implications for mud removal in near-field river mouth discharges. J. Geophys. Res. Oceans 121, 2142–2162.

Sullivan, P.P., McWilliams, J.C., 2010. Dynamics of winds and currents coupled to surface waves. Annu. Rev. Fluid Mech. 42, 19–42.

Sullivan, P.P., McWilliams, J.C., Moeng, C.H., 1994. A subgrid-scale model for large-eddy simulation of planetary boundary-layer flows. Bound.-Layer Meteorol. 71, 247–276.

Tejada-Martinez, A., Grosch, C., 2007. Langmuir turbulence in shallow water. part 2. large-eddy simulation. J. Fluid Mech. 576, 63–108.

Umlauf, L., Burchard, H., Hutter, K., 2003. Extending the k–ω turbulence model towards oceanic applications. Ocean Model. 5, 195–218.

Van Roekel, L., Adcroft, A.J., Danabasoglu, G., Griffies, S.M., Kauffman, B., Large, W., Levy, M., Reichl, B.G., Ringler, T., Schmidt, M., 2018. The kpp boundary layer scheme for the ocean: Revisiting its formulation and benchmarking one-dimensional simulations relative to les. J. Adv. Model. Earth Syst. 10, 2647–2685.

Van Roekel, L., Fox-Kemper, B., Sullivan, P., Hamlington, P., Haney, S., 2012. The form and orientation of langmuir cells for misaligned winds and waves. J. Geophys. Res. Oceans 117.

Verney, R., Lafite, R., Brun-Cottan, J.C., Le Hir, P., 2011. Behaviour of a floc population during a tidal cycle: laboratory experiments and numerical modelling. Cont. Shelf Res. 31, S64–S83.

Warner, J.C., Sherwood, C.R., Arango, H.G., Signell, R.P., 2005. Performance of four turbulence closure models implemented using a generic length scale method. Ocean Model. 8, 81–113.

Warner, J.C., Sherwood, C.R., Signell, R.P., Harris, C.K., Arango, H.G., 2008. Development of a three-dimensional, regional, coupled wave, current, and sediment-transport model. Comput. Geosci. 34, 1284–1306.

Winterwerp, J.C., 1998. A simple model for turbulence induced flocculation of cohesive sediment. J. Hydraul. Res. 36, 309–326.

Yoshikawa, Y., Baba, Y., Mizutani, H., Kubo, T., Shimoda, C., 2018. Observed features of langmuir turbulence forced by misaligned wind and waves under destabilizing buoyancy flux. J. Phys. Oceanogr. 48, 2737–2759.

Yu, W., Song, J.B., Cao, A.Z., Yin, B.S., Guan, S.D., 2018. An improved second-moment closure model for langmuir turbulence conditions: Model derivation and validation. J. Geophys. Res. Oceans 123, 9010–9037. doi:10.1029/2018JC013878.

Yuan, J., Liang, J.H., 2021. Wind- and wave-driven ocean surface boundary layer in a frontal zone: Roles of submesoscale eddies and ekman–stokes transport. J. Phys. Oceanogr. 51, 2655–2680.

List of Tables

Table 1: Model configuration for 1DV model simulations. Hyphen (—) denotes processes that are excluded.

Case	SMC Model	Wave breaking	Flocculation Processes
1DVa	modified $k-\omega$ (Yu et al., 2018)	Included	Included
1DVb	standard $k-\omega$ (Umlauf et al., 2003)	Included	Included
1DVc	standard $k-\omega$ (Umlauf et al., 2003)	—	Included
1DVd	modified $k-\omega$ (Yu et al., 2018)	Included	—

Table 2: Parameters of sediment flocs used in the model.

Class of Flocs	Diameter [μm]	Density [$\mathrm{kg\,m^{-3}}$]	Settling velocity [$\mathrm{mm\,s^{-1}}$]
1	4.0	2600.0	0.0134
2	5.7	2138.7	0.0189
3	8.0	1812.5	0.0268
4	11.3	1581.8	0.0379
5	16.0	1418.8	0.0536
6	22.6	1303.4	0.0758
7	32.0	1221.9	0.1072
8	45.3	1164.2	0.1516
9	64.0	1123.4	0.2144
10	90.5	1094.6	0.3032
11	128.0	1074.2	0.4288
12	181.0	1059.8	0.6064
13	256.0	1049.6	0.8575
14	362.0	1042.4	1.2127
15	512.0	1037.3	1.7151
16	724.1	1033.7	2.4255
17	1024.0	1031.2	3.4302
18	1448.2	1029.4	4.8510
19	2048.0	1028.1	6.8603

List of Figures

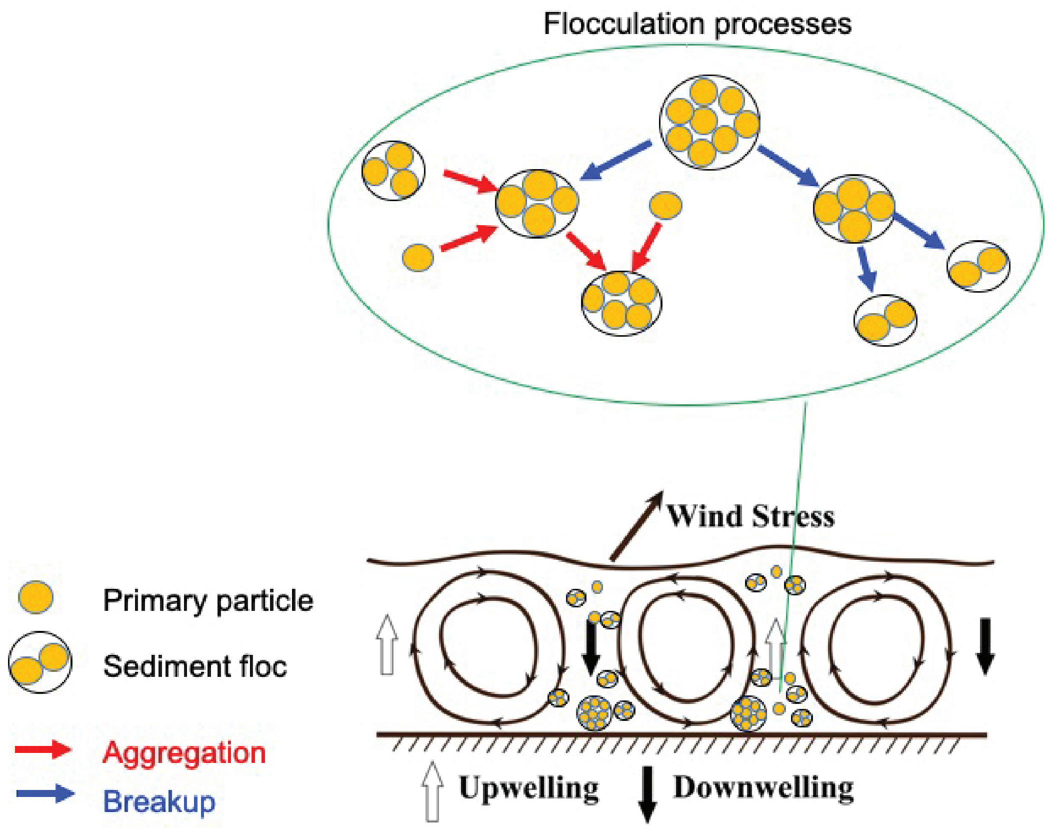

Figure 1: Schematic for flocculation processes (aggregation + breakup) of cohesive sediments in Langmuir turbulence.

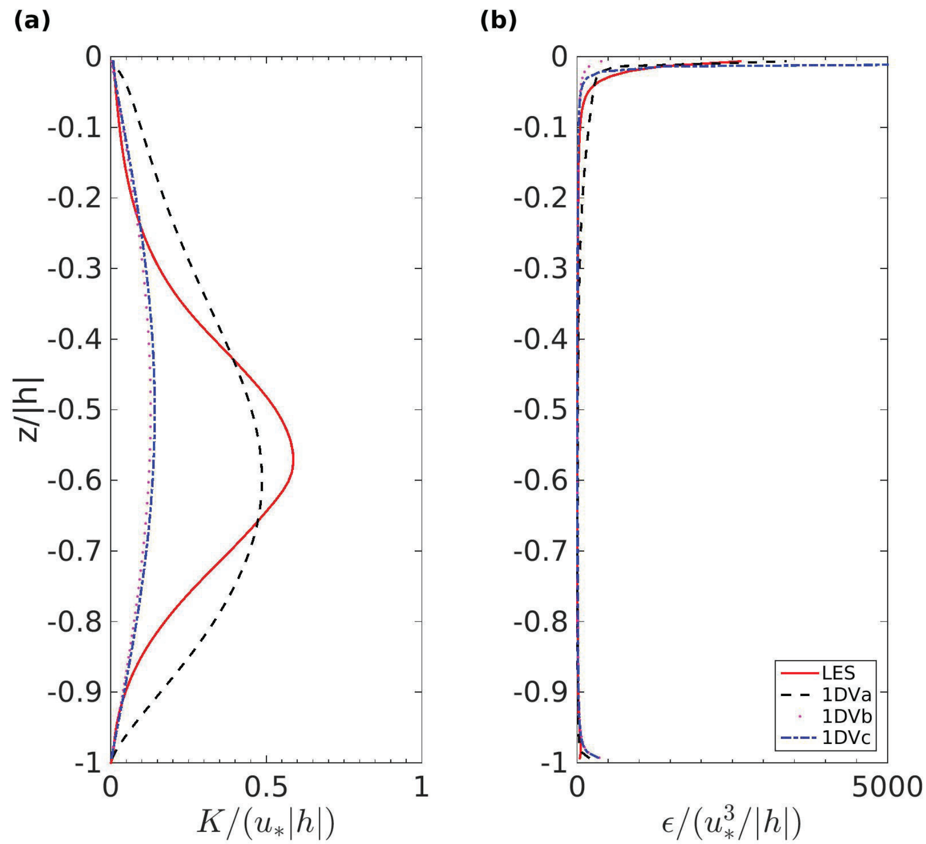

Figure 2: Vertical profiles of (a) normalized eddy viscosity ($K/(u_*|h|)$) and (b) normalized turbulent kinetic energy dissipation rate ($\epsilon|h|/u_*^3$) from: LES (red solid), Case 1DVa (black dashed), Case 1DVb (magenta dotted), and Case 1DVc (blue dash-dotted).

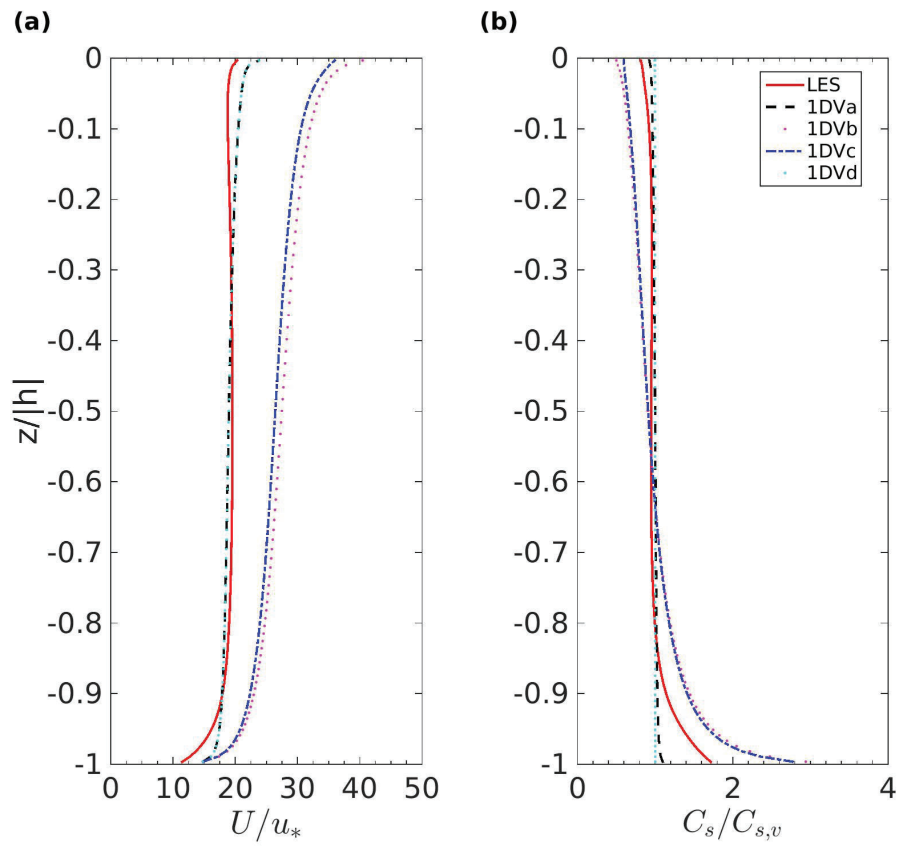

Figure 3: Vertical profiles of (a) normalized mean horizontal velocity (U/u_*) and (b) normalized total floc mass concentration ($C_s/(C_{s,v})$) from: LES (red solid), Case 1DVa (black dashed), Case 1DVb (magenta dotted), Case 1DVc (blue dash-dotted), and Case 1DVd (cyan dashed).

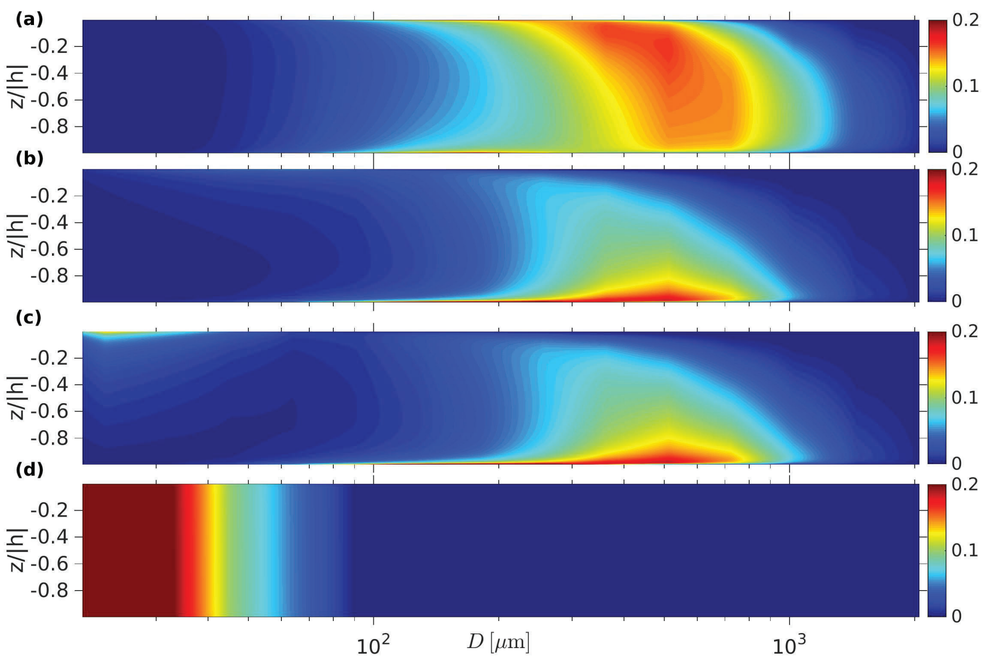

Figure 4: Vertical profiles of floc mass density [$gL^{-1}(ln(D_{k+1}) - ln(D_k))^{-1}$, where D_k is the diameter of floc in size class k] in 1DV model: (a) Case 1DVa, (b) Case 1DVb, (c) Case 1DVc, and (d) Case 1DVd.

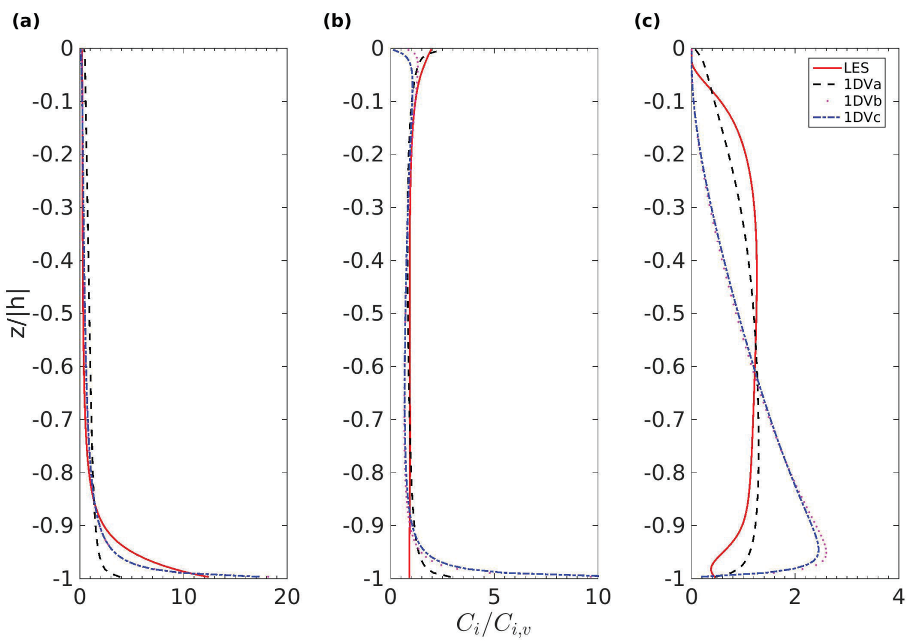

Figure 5: Vertical profiles of normalized floc mass concentration ($C_i/(C_{i,v})$) of size (a) $D = 4.0\,\mu$m, (b) $D = 128.0\,\mu$m, and (c) $D = 1024.0\,\mu$m from: LES (red solid), Case 1DVa (black dashed), Case 1DVb (magenta dotted), and Case 1DVc (blue dash-dotted)

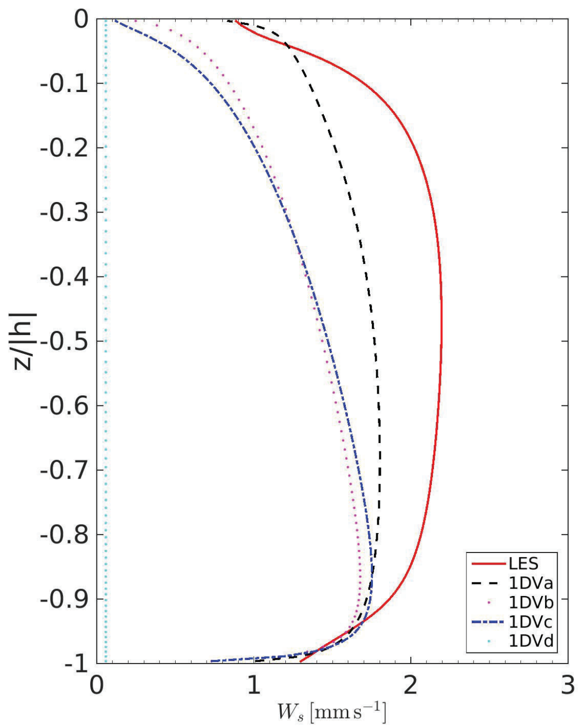

Figure 6: Comparison of vertical profiles of mass weighted settling velocity (W_s [$\mathrm{mm\,s^{-1}}$]) between LES model (red solid) and 1DV model (black dashed).